IEEE Access
Multidisciplinary ⋮ Rapid Review ⋮ Open Access Journal

Received September 13, 2020, accepted September 24, 2020, date of publication September 28, 2020,
date of current version October 8, 2020.

Digital Object Identifier 10.1109/ACCESS.2020.3027205

3D Correspondence and Point Projection Method for Structures Deformation Analysis

AURELIO G. MELO[1], (Member, IEEE), MILENA F. PINTO[2], (Member, IEEE), LEONARDO M. HONÓRIO[1], FELIPE M. DIAS[1], AND JULIANO E. N. MASSON[3]

[1]Department of Electrical Engineering, Federal University of Juiz de Fora, Juiz de Fora 36036-900, Brazil
[2]Department of Electronics Engineering, Federal Center for Technological Education of Rio de Janeiro, Rio de Janeiro 20271-110, Brazil
[3]Department of Automation and Systems, Federal University of Santa Catarina, Florianópolis 88040-900, Brazil

Corresponding author: Leonardo M. Honório (leonardo.honorio@ufjf.edu.br)

This work was supported by Coordenação de Aperfeiçoamento de Pessoal de Nível Superior (CAPES), Conselho Nacional de Desenvolvimento Científico e Tecnológico (CNPq), Institutos Nacionais de Ciência e Tecnologia (INCT)–Instituto Nacional de Energia Elétrica (INERGE), BAESA, ENERCAN, and FOZ DO CHAPECÓ, under the supervision of Agência Nacional de Energia Elétrica (ANEEL)-The Brazilian Regulatory Agency of Electricity, under Project PD 03936-2607/2017.

ABSTRACT Mining slopes, electrical power generation dams and several big construction enterprises demands continuous inspections. The size and diversity of these structures demands high precision and portable approach. In such environments, 3D reconstruction methodologies are able to capture and analyze the real world in detail. However, the accuracy and precision can affect the ability to process and interpret the acquired data. For instance, laser scanning is a very accurate method and can deliver a higher quality result. Meanwhile, 3D photogrammetry using a single camera and Structure From Motion (SFM) have their performance correlated with the image quality. In a typical application, 3D data from reconstruction is pre-processed by a specialist. Then, it is stored for comparison and analyzed over time. The posterior analysis has several challenges associated with the reconstruction process characteristics. Several techniques have been developed to allow the comparison of point cloud captured at different epochs. Therefore, this research work presents a new methodology to perform alignment and comparison of point clouds, namely 3D-CP2, an acronym for 3D Correspondence and Point Projection. This method intends to analyze the point cloud motion to be applied in terrestrial 3D SFM reconstructions. Besides, the technique can also be used in many other related applications. The methodology developed in this work is applied in controlled experiments and real use cases to show its potential for point cloud displacements analysis. The results showed that the proposed method is efficient and can produce results more accurately than the referenced literature.

INDEX TERMS Aerial inspection, point cloud change detection, structural analysis, structure from motion, 3D reconstruction.

I. INTRODUCTION

Massive constructions are typically associated with high contingency risks demanding the highest security and inspection standards [1]. If slopes and dams are considered, the catastrophic disruption consequences and the enormous forces that act on these structures make those structures especially critical, demanding strict inspections. Among all types of inspection categories, the 3-dimensional Surface Deformation Analysis (SDA) [2] is one of the significant importance. The SDA requires a very dense Geo-referenced point-cloud where each point must be compared with its correlative from previous inspections to find any possible displacement. Several challenges arise from the point cloud deformation analysis that remains unsolved despite the increasing number of developed methods to detect and quantify displacement and deformation [3], [4]. Besides, many applications can benefit from morphological surface data [5], [6]. For instance, erosion, sedimentation, and other environmental factors may reshape structures and create risks to people as well as to the environment [7], [8]. The structural deformation monitoring requires constant tracking, and the rate of change can be regularly measured to estimate structure stability and safety. However, due to the lack of regular structures and smooth objects, the deformation analysis of natural scenes is particularly demanding for point cloud since two points cannot be readily identified in different epochs [9].

In the last years, many different technologies have been proposed for inspecting structures deformation. For example, Light detection and ranging (LIDAR), 3D Cameras,

The associate editor coordinating the review of this manuscript and approving it for publication was Chunbo Xiu.

and Structure From Motion (SFM) have been deployed in many modern applications, as can be seen in [10]–[15]. Note that in these mentioned applications, the 3D point clouds are generated representing the objects and places over inspection. However, they generate large amounts of data related to the surface of a given area, requiring sophisticated engineering tools to extract useful information.

There are many challenges associated with processing this kind of information [16], [17]. As an example, a point in two different epochs reconstruction may not be reconstructed in one of the epochs. Another issue is the amount of texture and quality of the reconstruction that can create false correspondences. Figure 1 depicts these common issues related to point cloud reconstruction. In Figure 1(a), the reconstructions have different point density. Thus, the matching process corresponds to the surfaces with different scales, which make one of them wrong in relation to the real-world. Figure 1 (b) shows that reconstructions errors in the surface detail can make a typical stair surface looks like a straight line.

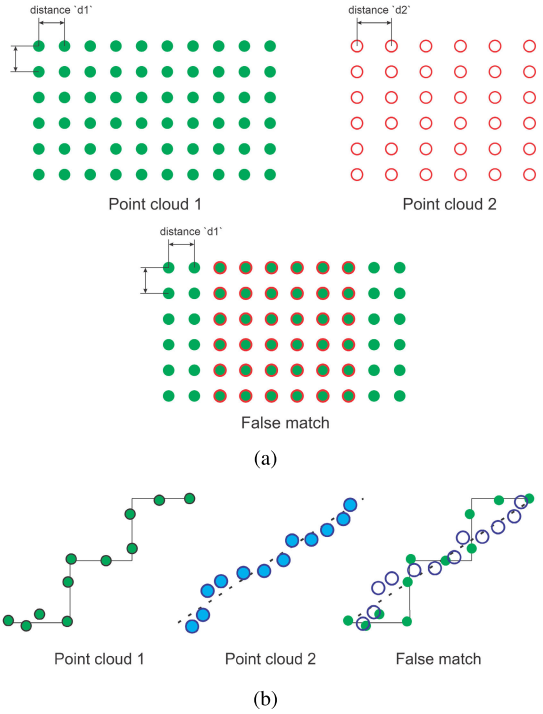

FIGURE 1. Common issues in the point cloud reconstruction. (a) A point is not identified. (b) False correspondence due poor quality of the reconstruction.

Other difficulties related to the point clouds can be associated with the methods employed to compare them. Many methods, such as cloud-to-cloud (C2C) [18] and multi-scale model-to-model cloud (M3C2) [10], use the normal of the surface to evaluate point cloud distance. Despite being efficient in many cases, these methods are sensible in situations where the movement is larger or happens in a different direction from the surface normal. As a solution to these issues, several techniques have been developed over the years, such as in [19]. As stated by the authors of Qin *et al.* [20], the two major approaches in 3D change detection are the methods that rely on statistical analysis to find correlations among data, and the methods that use surface reconstruction to collapse the point cloud to an average position. However, these solutions have limitations and may not produce accurate results.

Despite these limitations, these methods are still used and applied in research papers. In [21], the authors used M3C2 to perform an analysis of rockfall evaluating the characteristics of the method. The authors in [22] combined M3C2 with statistical methods to determine areas of erosion, and in [14], the method was used to evaluate the effect of different changes in the SFM method. In summary, many applications can benefit from more precise and accurate measurement methods.

A. MAIN CONTRIBUTIONS

Therefore, this research work proposes an innovative solution to find correspondence among SFM reconstructions. From these correspondences, the process estimates cameras' alignment. Once images are aligned, the points can be projected among both images, and correspondences among groups of 2D and 3D points can be calculated. Then, it is possible to estimate the motion direction as well as to find a proper alignment between patches of two point clouds. An appropriate subtraction of the point clouds is performed using traditional methods to determine the scalar difference and the respective displacement for each point. The proposed method is called 3D Correspondence and Point Projection (3D-CP2). This research uses experimental data from a series of controlled experiences and real conditions to demonstrate the good performance of the 3D-CP2 methodology. The contributions of this research can be summarized as follow:

- A proposition of an innovative method for estimating point cloud movements or deformation based on 2D/3D correspondence and point projection.
- Analysis of methods performance using a controlled environment and data of real structures.

B. ORGANIZATION

The remainder of this work is organized as follows. Section II presents a brief review of related works, highlighting the state-of-the-art in point cloud alignment process. Section III details the proposed methodology and its mathematical foundations. Section IV shows the proposed experiments with a proper discussion of the results. The concluding remarks and future work are conducted in Section V.

II. BACKGROUND AND RELATED WORKS

Point clouds are increasingly used in many applications. As an example, the autonomous navigation system used in cars and drones is becoming very reliant on depth cameras, radar, or laser [23]. Other prominent applications include precision agriculture [24], terrain analysis [25], and structural inspection [26]. Note that all those applications generate a

large sum of data related to the surface of the objects. Thus, a common requirement to process all geometric information is the alignment between two point clouds.

Several studies have evaluated the accuracy of modern remote sensing techniques. In the works of Qin *et al.* [20] and Lindenbergh and Pietrzyk [27], the authors presented a theoretical background of 3D point cloud change detection. There are two major deformation models, that is, point-based and surface-based. The point-based approach is used to compare the point clouds directly, and the most used methods are the C2C and M3C2 algorithms [10]–[28]. Other methods, such as surface-based models, including cloud-to-mesh (C2M) and mesh-to-mesh (M2M), reconstruct a triangle mesh surface from a given point cloud. Then, the resulting meshes are compared, as demonstrated in Wang *et al.* [29].

A significant drawback of the point-based and surface-based models is the inability to correctly estimating the plane deformations, which is explained by how these methods find the correspondences among points in different reconstructions epochs for displacement estimation. For instance, the surface-based process searches the correspondent point in the direction of the normal vector of the underlying surface or a plane fitted to the neighboring points. The point-based approach selects the particular nearest point from the other epoch [10]–[13].

Another challenge is the automatic point cloud registration process [30], [31]. In the work of Park *et al.* [32], the authors used registration to combine point clouds in such a way that they generate larger scenes. This use of point cloud registration is widespread when performing reconstruction of architectonic areas. For terrestrial data analysis or inspection, the registration process has to find at least three control points that are in the same position on both point clouds to find the alignment between them.

Among algorithms that find alignment between point clouds, the Iterative Closest Point (ICP) is a commonly used method [33]. This is an iterative algorithm where the Mahalanobis distance between the point clouds are minimized by a series of random point selections and transformations. There are many variations of the ICP method, as can be seen in Shi *et al.* [34], Ren *et al.* [33], and Bouaziz *et al.* [35]. Note that the ICP method is adopted in a few point cloud tools, such as Cloudcompare [36]. Despite the use, its application requires a skilled operator due to the method's shortfalls. It requires that the point cloud positions are close to each other, where the process only finds the final transformation.

Note that the correspondences are crucial for 3D registration. Several works have focused on the design of 3D features to capture local geometry for correspondence establishment. The works of Wagner *et al.* [37] and Rethage *et al.* [38] proposed the use of local feature descriptors to find the correspondences. However, most of the methods found in the literature require highly specialized personnel to select the proper point cloud parts to be compared, aligned, and to analyze them.

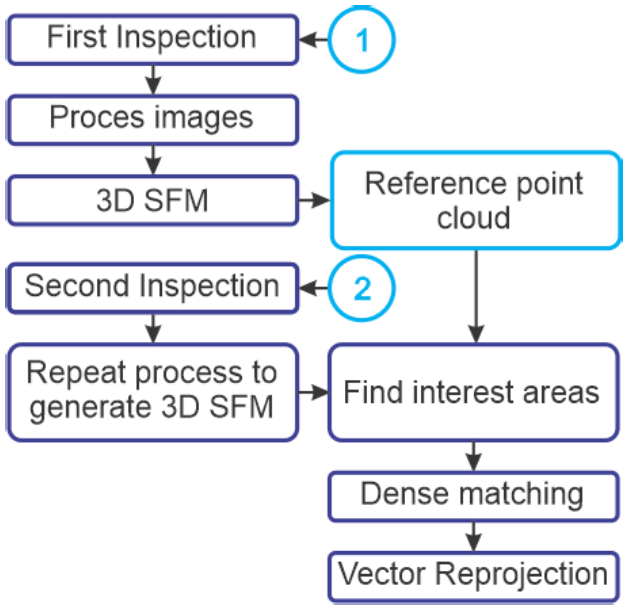

FIGURE 2. Flowchart of the 3D-CP2 methodology.

In this sense, the current methods present difficulties in being deployed in real-world applications. Therefore, the correspondence methodology proposed in this work can improve the efficiency of existing processes dramatically. These improvements are expected by eliminating the need for manual point cloud alignment, determination of movement in the real deformation direction instead of the normal direction of the surface, and accurate movement measurement when the object position changes significantly regarding the point cloud size.

III. PROPOSED 3D DEFORMATION ANALYSIS

This section details the proposed method and its mathematical foundations for analyzing the deformation of 3D reconstructions. Figure 2 presents a global overview of the 3D-CP2 methodology. Initially, a first inspection is performed, and the point clouds are generated. Therefore, this cloud becomes a reference for future point clouds from this same inspected area. After generating a point cloud for a second inspection, the point of interest is found, and a dense matching process is performed. Finally, the algorithm makes the new projection of the point vector.

A. PROBLEM STATEMENT

Given two sets of input images from different inspections $O^t = \{\boldsymbol{I}_1^t, \boldsymbol{I}_2^t, \ldots, \boldsymbol{I}_k^t\}$ and O^{t+1}, obtained at inspections t and $t+1$, respectively. From these image sets, it is assumed that is possible to apply SFM to reconstruct two point clouds sets $N^t = \{\boldsymbol{p}_1^t, \ldots, \boldsymbol{p}_k^t\}$ and N^{t+1}, where the first point cloud N^t is called reference cloud and $\boldsymbol{p}_i^t$ is the i-th point in the reference cloud. The second point cloud and image sets, O^{t+1} and N^{t+1}, are the candidate sets. Note that the images can't be directly analyzed for deformation after the point clouds generation.

In the next step, correspondences among the reference and candidate images are determined to build images pair. In other words, for each image $\boldsymbol{I_k^t}$ in reference set O^t, a pair image $\boldsymbol{I_k^{t+1}}$ is determined in the candidate set O^{t+1}. A measurement distance has to be defined to determine which image in the candidate set is the right pair in the reference set. The next paragraph presents the variables to determine this distance, along with proposed distance measurements.

Note that a set of parameters needs to be determined to estimate the correlation between two images. For this, it is possible to use the models generated for each image during the SFM point cloud generation stage, as shown in [14]. For each image I_k^x in the O^x, an extrinsic set of camera parameters $\boldsymbol{C}_k^x[\boldsymbol{R_C}|\boldsymbol{T_C}]$ is calculated. The matrix $\boldsymbol{C}_k^x$ is comprised by a rotation matrix $\boldsymbol{R_C}$ and a translation vector $\boldsymbol{T_C}$ that accurately represent the camera position in the point cloud $\boldsymbol{N}^x$ reconstruction space. Observe that a calibration stage is required to minimize those issues if lens errors or other image deformation Then, it is possible to estimate the error between two images, $\boldsymbol{I_k^t}$ and $\boldsymbol{I_{h_k}^{t+1}}$, as a distance $dist = e(\boldsymbol{I_k^t}, \boldsymbol{I_{h_k}^{t+1}})$ in relation to sum of the position and rotation errors in the camera parameters, as presented in Equation 1 [39].

$$dist = \frac{||\boldsymbol{c_k^{t+1}} - \boldsymbol{c_k^t}||}{||\boldsymbol{c_k^t}||} + \cos^{-1}\left(\frac{\text{trace}(\boldsymbol{R_k^t}\boldsymbol{R_{h_k}^{t+1}}) - 1}{2}\right) \quad (1)$$

Based on these measurements, a set of images is selected as a pair. This pairwise selection can be represented by the set $W = \{(\boldsymbol{I_1^t}, \boldsymbol{I_1^{t+1}}), (\boldsymbol{I_2^t}, \boldsymbol{I_2^{t+1}}), \ldots, (\boldsymbol{I_{L^t}^t}, \boldsymbol{I_k^{t+1}})\}$. Figure 3 depicts this process. It is important to note that the distance in a given pair of image $(\boldsymbol{I_1^t}, \boldsymbol{I_1^{t+1}})$ certainly effects the final results of the algorithms. For this reason, in an ideal situation, these distances should be kept as close as possible among subsequent inspections to limit errors.

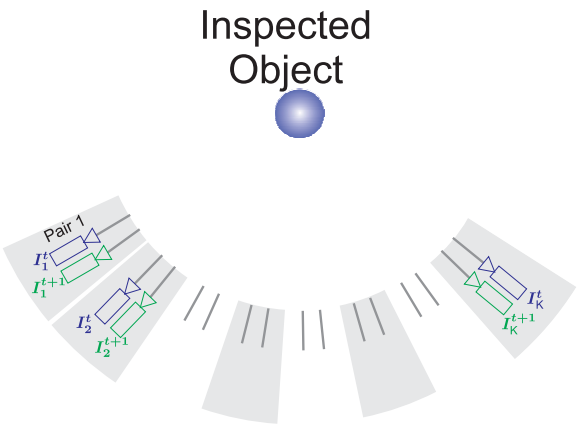

FIGURE 3. Experiment layout representation.

After alignment a dense set of points $\boldsymbol{p_i^t}$, a point is projected in all visible images. After this projection in the k-th image of the first inspection set O^t, the pair images $\boldsymbol{I_k^t}$ and $\boldsymbol{I_k^{t+1}}$ of the set W are selected. Then, dense matching is applied to find correspondences between groups of points in the pair images. The correspondences are denominated $\boldsymbol{\omega_u^{i,h_k,th_1,t+1}}$.

The next step in the algorithm is the selection of the 3D points $\boldsymbol{p_j^{t+1}}$ from the cloud N^{t+1}. The points are selected if their projections $\boldsymbol{I_k^{t+1}}$ are within a maximum distance th_2 from the points $\boldsymbol{\omega_u^{i,h_k,th_1,t+1}}$. For all points in the 3D projection at a given distance th_2 and a median $\boldsymbol{d_i^{k,t}}$, the distance for the correspondent points is estimated. The estimated median represents the movement performed by the group of points.

Figure 4 exemplifies the correspondence process determination for the point $\boldsymbol{p_i^t}$ from the k-th image of the inspection O^t. As aforementioned, the median $\boldsymbol{d_i^t}$ represents the point movement vector $\boldsymbol{p_i^t}$. A limit from a given point $\boldsymbol{p_i^t}$ can be defined to maximize efficiency in a maximum distance, which is defined as d_{max}. However, this distance also limits the amount of movement that can be detected. Therefore, it has to be carefully estimated for each cloud-based on the reconstruction scale.

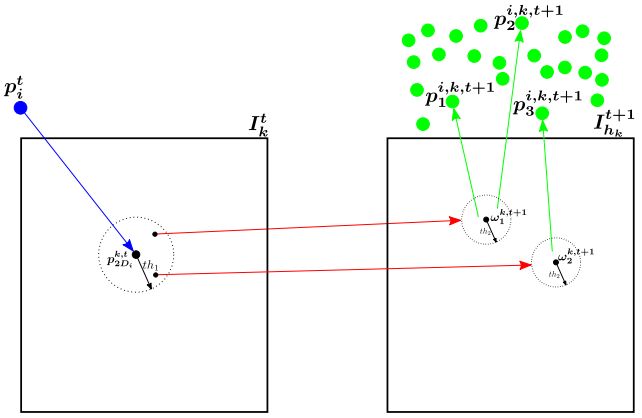

FIGURE 4. Correspondence estimation for the i-th 3D point of N^t using the k-th image of the inspection set W.

After this process, the algorithm determines each point's position from the first image concerning the second one. As can be seen, this information allows a precise movement estimation for each point in the cloud. The distance can be calculated using any methods from the literature, such as Euclidean distance. However, it is essential to note that reconstruction errors in the SFM process can affect the results. Thus, the filtering process is still required to reduce errors.

All the processes described in this section can be summarized in Algorithm 1. This algorithm details the input and outputs of the method as well as the processing steps. However, note that the stages to perform the SFM reconstruction were omitted once they are dependent on the user software, which is outside of this research scope.

Figure 5 presents the data flow from Algorithm 1. The first image set (from initial inspection) is presented at the left, and the second image set is at the right of the diagram. The SFM process is applied to both image sets, and a registration process is performed to align both point clouds. Note that image pairing finds the matches among those images using image descriptors and point cloud data. This last step output is to feed into the 2D-2D match, and latter to the 3D-3D

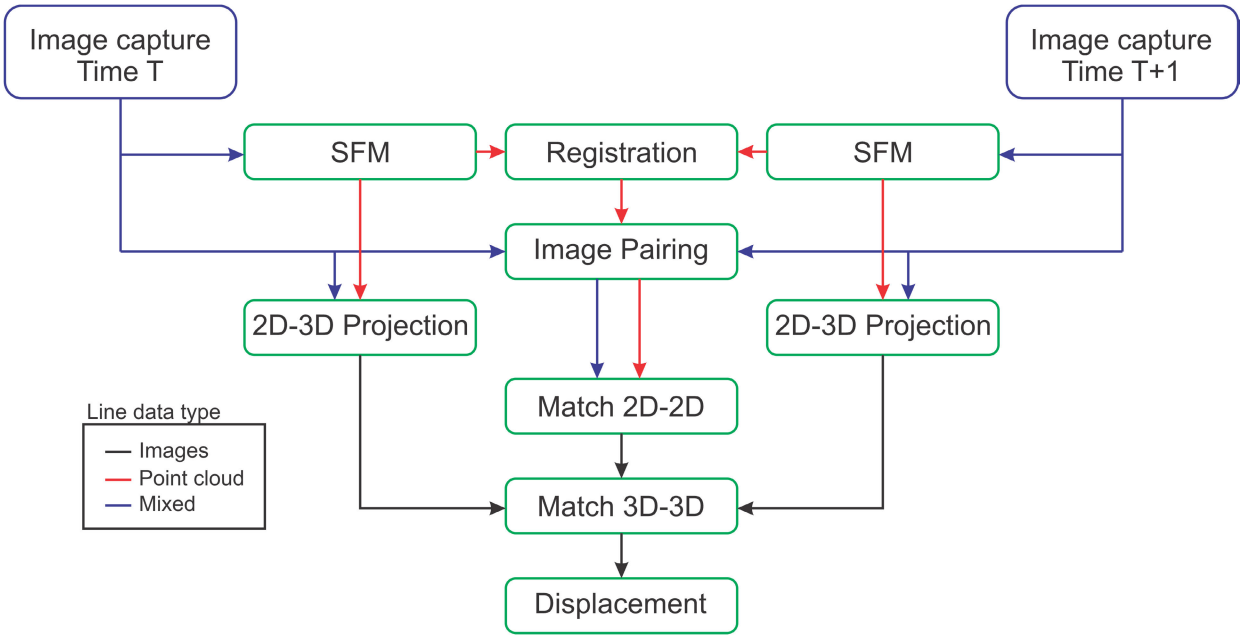

FIGURE 5. Infographic representation of the processing steps.

Algorithm 1 3D-CP2 Algorithm

Input: 3D Point cloud 1 (ptc1), Images for reconstruction 1;
Input: 3D Point cloud 2 (ptc2), Images for reconstruction 2,
camera calibration files;
1: Perform registration for ptc1 and ptc2;
2: Find pair of images, i.e. images that are correspondents;
3: Perform reprojection of points from ptcX to images (2D-3D Projection);
4: Find points correspondences (2D-2D);
4: Perform match (3D-3D);
5: **for** each correspondece 3D-3D in the point cloud
6: Estimate distance between points;
7: **end**
8: Estimate scalar field as output;
Output: Reference file with movement of each point;

match. The last stage also uses information from the 2D-3D reprojection of the SFM points in the image set. The 2D/3D reprojection finds where each 3D point land is in the input images. At last, the distance among 3D points matches is estimated.

Figure 6 presents a complete overview of the process, once many steps of 3D-CP2 are complex and difficult for visualizing. First, in Figure 6 (a), a set of pictures is taken from the inspected site (Figure 6 (b)). An SFM process produces the 3D point cloud (Figure 6 (c)), generating a reconstruction showed in Figure 6 (d). The reconstruction has to be cleaned, i.e., vegetation and other changing parts have to be removed to avoid errors resulting in Figure 6 (e). This process has to be repeated for the second inspection to a later comparison. The picture set from both reconstructions and their respective point clouds is used as input for the algorithm. The figures are matched and form pairs, as illustrated in Figure 6 (f). The points are re-projected (6 (g)) and matched (6 (h)). Then, the last step estimates the distance from matched points using an appropriated metric. Note that the image paring described in Figure 6 (f) uses descriptors. These descriptors are essential to allow the recognition of unique features in each image that is somewhat invariant to luminosity, position, and orientation. Thus, the descriptors estimation performance defines the method ability to identify environment characteristics as well as to form image pairs. If this pairing stage is not successful, the subsequent stages may induce errors in the final distance estimation.

As can be seen, the displacements are calculated from 3D-3D matches, which ensures that the point in the second 3D point cloud is the same from the first 3D point cloud. This process will be able to estimate the real movement of the point. This is the essential advantage of the proposed method, once most methods will estimate the movement in the normal direction, which may not represent reality. The steps are taken using re-projection from the images to the points clouds also ensures that the individual points are the same from the images. This is an advantage over methods that rely on point cloud match only.

IV. RESULTS AND DISCUSSIONS

A. MATERIALS AND METHODS

This section presents two sets of experiments to evaluate the 3D-CP2 methodology. The first set was performed in a controlled environment to determine the algorithm efficiency in

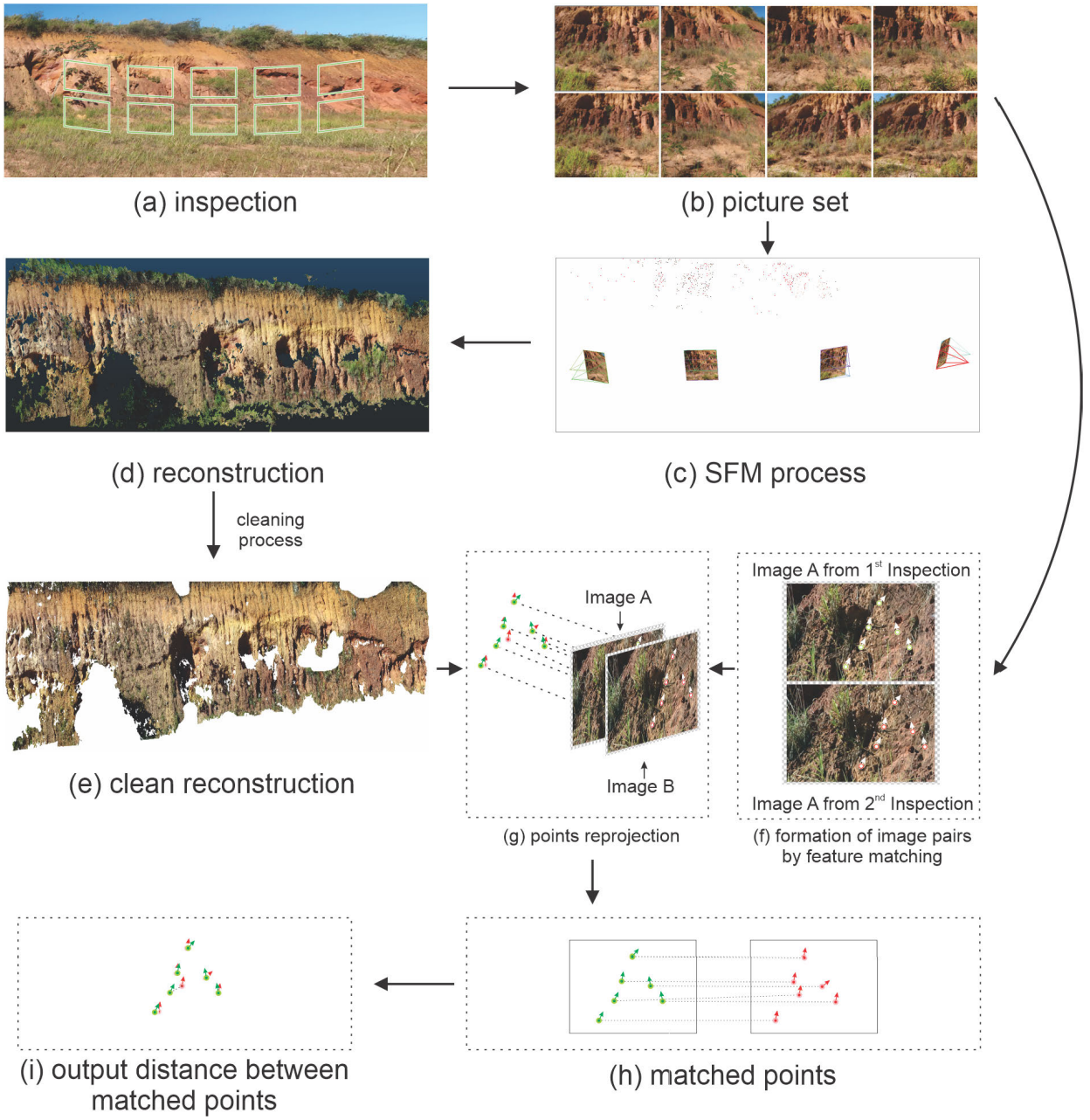

FIGURE 6. Infographic representation of the processing steps.

specific cases. The second set was comprised to analyze real cases of terrain deformation. These controlled experiments aim to establish the algorithm's efficiency and accuracy in relation to the ground truth and the methods in the literature. The tests were carried out to compare the 3D-CP2 with the M3C2 technique proposed by Lague *et al.* [40], which is considered state-of-the-art in the 3D cloud deformations' estimation.

As previously explained, this controlled environment was selected to minimize external influence and establish the measurements concerning the ground truth. Note that other variables, such as luminosity and occlusion, and a set of fixed camera positions, were selected to decrease the comparison errors. Besides, the dimensions of the boxes in the experiments are known (i.e., 245 mm x 175 mm). These measures were used to make the real scale of the reconstructions. Also, six images with 4864 x 3648 px resolution were used to perform the scenes reconstructions.

The experiments considered movements in different angles concerning the normal of the surface once many methods in the literature use the normal of the point clouds to analyze the deformation and to estimate distances. Figure 7 shows a representation of the movements performed in the first set of experiments. In the first experiment,

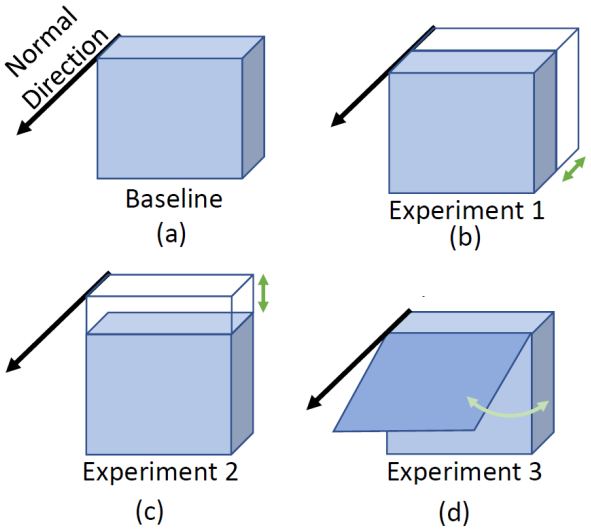

FIGURE 7. Movements performed in the first set of experiments. (a) Baseline. (b) Movement on normal direction. (c) Perpendicular movement in relation to normal direction. (d) Angular movement in relation to normal.

Figure 7 (b), the movement is in the normal direction of the surface. This is an easy case for all methods. The second and third cases, which are presented in Figure 7 (c) and Figure 7 (d), respectively, are in different angles, making it difficult a proper movement estimation.

B. RESULTS IN A CONTROLLED SCENARIO

The first experiment was carried considering the movement in the normal direction presented in Figure 7 (a). Figure 8 (a) presents the box attached to the wall and Figure 8 (b) shows the same box with a 40 mm displacement from it. The box position was carefully determined in both situations to reduce the measurement errors to less than 1mm.

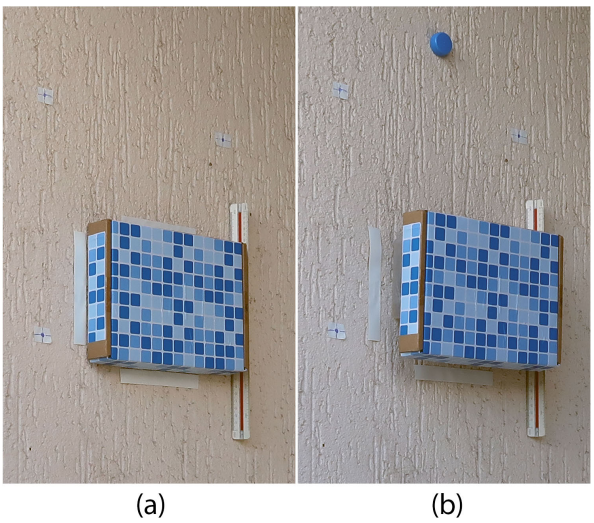

FIGURE 8. Movement performed in the normal direction of the surface. (a) Initial position. (b) Displaced position.

Through the use of the photographic inspection a set of images was built and is represented in Figure 8. In the experiment, carefully selected marks are positioned to determine the scale and improve the SFM process by providing a reference control point. In real situations, if it is unfeasible to use those markings, real-time kinematics or post-processing kinematics should be considered to allow a very precise result. Note, however, that this will also improve the performance of other methods, such as M3C2, and should always be considered. Using the image-sets, the SFM reconstructions were obtained as shown in Figure 9 (a) and 9 (b), respectively. Using those reconstructions it is possible to estimate the point cloud distance by applying the M3C2 algorithm. The M3C2 result was overlaid in the Figure 9 (c).

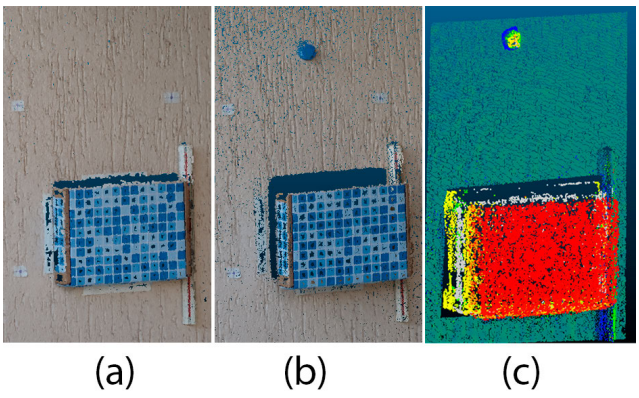

FIGURE 9. SFM reconstructions. (a) Reconstruction of the baseline. (b) Reconstruction after normal movement. (c) Scalar representation of the distance.

Figure 10 (a), Figure 11 (a) and Figure 13 (a) present the point distances distribution for the 3D-CP2 method. The same procedure is performed for the M3C2 algorithm, which are shown in Figure 10 (b), Figure 11 (b) and Figure 13 (b). Note that for the normal movement, both histograms are similar in shape and distribution. This is the perfect situation for algorithms such as the M3C2. The method that relies on the normal of the surface to estimate the movement direction have its best performance in this kind of scenarios. For instance, if there were no errors in the calculations, only a single bar at 40mm with all the distance measurement points would be shown in the histogram.

The histograms of the perpendicular movement experiments, which are presented in Figure 11, are different from the last experiments. Figure 11 (a) has a similar distribution from the Figure 10 (a), but with some errors spread along the correct value. However, the M3C2 histogram of Figure 11 (b) shows two sharp spikes in values closer to zero. These errors in the M3C2 measurement occurred because this algorithm only perceives movement in the parts where there was no overlap. This is better detailed in Figure 12.

Note in Figure 12 that the upper part shows negative displacement. This negative displacement results from the normal direction being perpendicular to the surface and the

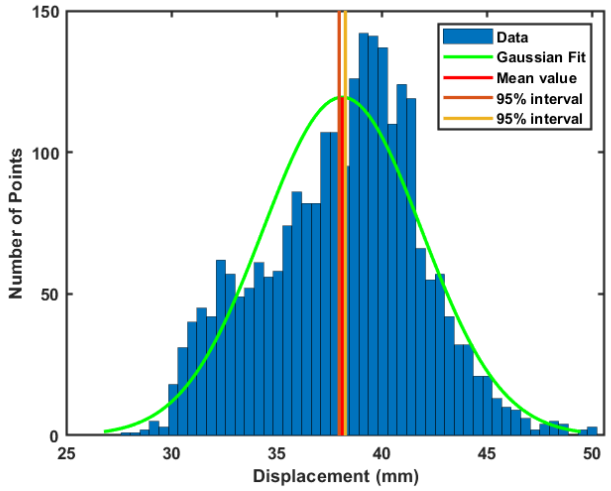

(a)

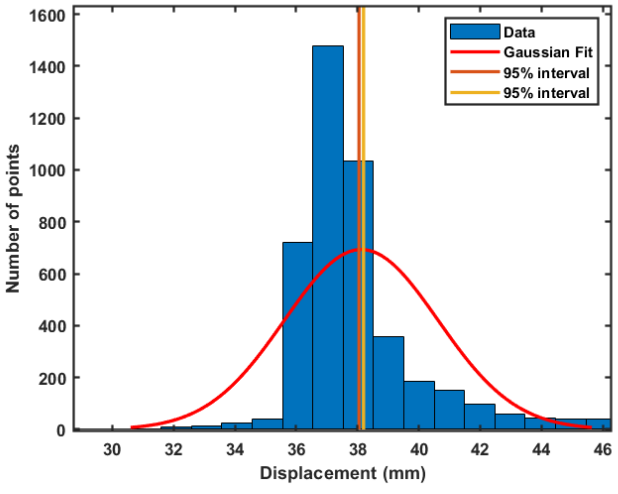

(b)

FIGURE 10. Histogram of points distances for movement in the normal direction. (a) 3D-CP2. (b) M3C2.

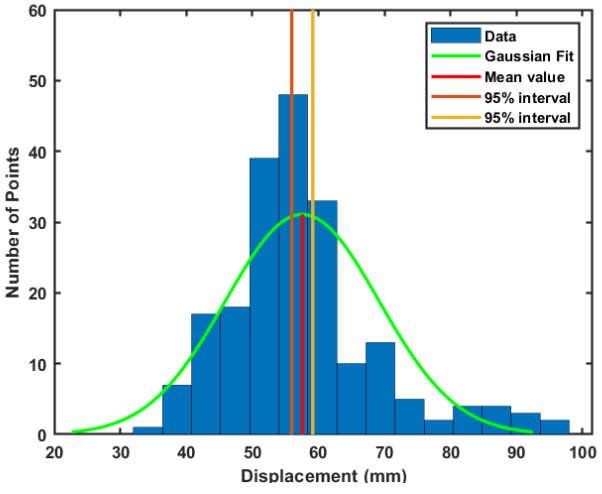

(a)

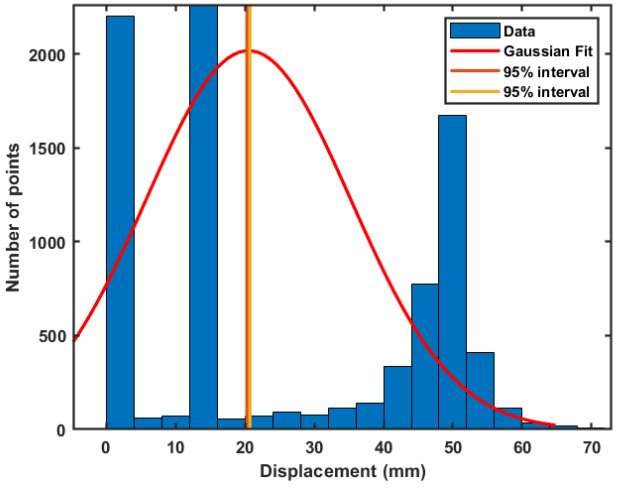

(b)

FIGURE 11. Histogram of points distances for movement in the perpendicular direction. (a) 3D-CP2. (b) M3C2.

box movement being in the perpendicular direction, exposing the surface. This is the same behavior from the bottom part of the box shown in red. The middle part of the box also shows some green points indicating zero displacements. The histograms did not include the wall surface at the sides of the box. In this sense, no point with zero displacements should be observed.

Figure 12 is a representation of the perpendicular movement experiment. In this Figure, a scalar field is overlaid to represent the distances calculated by the M3C2 algorithm. The scalar field uses the color blue to negative displacements, the color red to the positive displacements, and no displacements are in green. As can be seen, as the displacement is perpendicular to the normal of the surface, all calculations performed by the M3C2 are wrong. For instance, the negative displacement is the result of the M3C2 that estimates the movement in the direction of the absent board. In contrast, the real movement should be positive due to the box movement. This is the worst situation for the M3C2 algorithm, and the same behavior is also observed for every method that uses the normal direction in its calculations.

In this last experiment, the displacement has an angle about the normal of the surface. Figure 13 depicts the distance distribution for both 3D-CP2 and M3C2 methods. It is possible to observe in Figure 13 (b) that the M3C2 angles appear to be correct, showing an even distribution of distances, as expected for the box movement. However, Figure 14 illustrates the distance estimated by the M3C2 and the real expected distance.

As explained, the M3C2 estimates the distance using the normal of the surface as a reference to search for the points where it should find the next surface. This is represented in Figure 14 (a). It is possible to observe in Figure 14 (a) that the cylinder in the normal of the surface put the algorithm

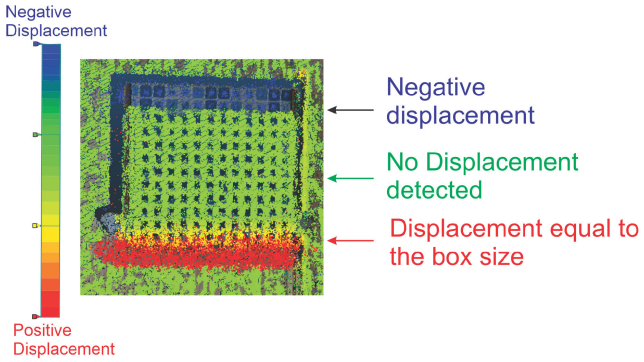

FIGURE 12. Representation of the M3C2 displacement as a scalar field.

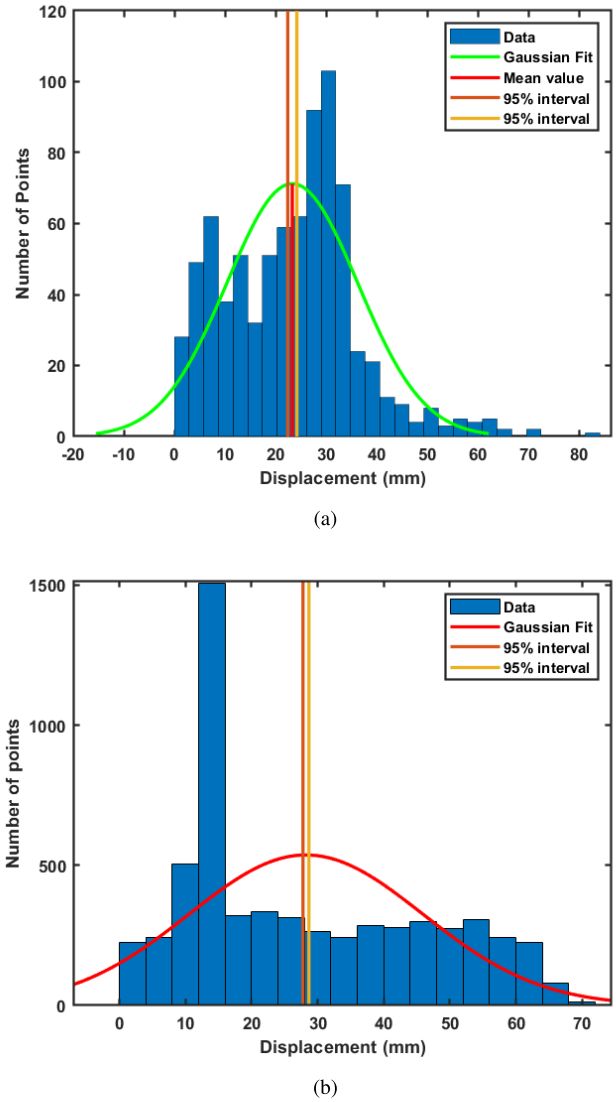

FIGURE 13. Histogram of points distances with an angle in relation to the normal of the surface. (a) 3D-CP2. (b) M3C2.

to a different point from the one where the surface has moved. The correct distance representation is presented in Figure 14 (b).

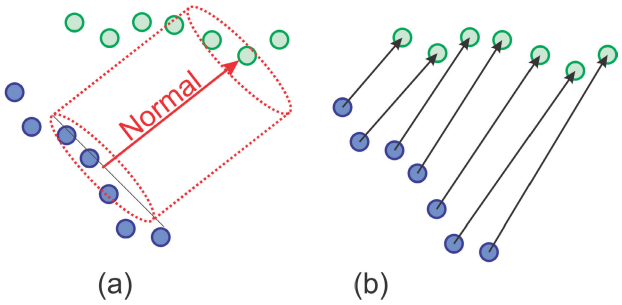

FIGURE 14. Movement estimation. (a) M3C2. (b) Correct movement.

Table 1 compiles the data from the histograms. This table also summarizes the mean values and standard deviation. It is possible to observe the 95% confidence interval for the data, allowing further analysis of its distribution.

These controlled results can provide an insight into the areas where the proposed methodology gives better results compared to the literature. As can be observed, the results obtained by methods that rely on the normal of the surface to compute displacements, such as C2M, and M3C2, can be misleading. These results may not represent the reality of the movement when it is not in the direction of the surface normal. They can provide a good insight into were movement happen. However, the scalar value of the change has to be subject to detailed inspection in each part of the surface.

C. CONTROLLED EXPERIMENTS IN REAL TERRAIN SURFACE

In the experiments performed in a controlled scenario, the texture of the surfaces was designed to provide a proper SFM reconstruction. In this sense, the second series of experiments were performed to show the potential of the algorithm in operating in real-world scenarios. In this second experiment, a series of pictures were taken on a hillside in two conditions. The first condition is the baseline, showed in Figure 15. In the second, a movement was applied in a rock on the hill in the normal direction. As already explained in the previous section, this direction is the best for the M3C2 algorithm. The normal direction was chosen because it does not put these methods into a disadvantage.

In this experiment, a set of five images from the each positions were taken. Figure 16 presents the SFM reconstruction generated for each scenario, and it represents the baseline. Both point clouds were manually scaled and aligned using the measurements taken at the scene.

The M3C2 algorithm was applied to the aligned point cloud generating a scalar field that represents the amount of movement measured. Figure 17 shows this result. Note that the point cloud density is not constant and it is affected by the vegetation, texture and luminosity of the scene. The negative and positive displacements are represented by the colors blue and red, respective. The areas with no displacements are represented by green.

TABLE 1. Data from the histograms summarizing the mean values and standard deviation.

	Mean value (mm)		Standard Deviation (p.u.)		95% confidence interval (mm)	
Experiment	1	2	1	2	1	2
Movement in the direction of the surface normal	38.134	38.1201	3.78	2.508	±0.148	±1.96
Perpendicular movement in relation to the surface normal direction	57.558	20.500	11.634	14.772	±1.598	±1.960
Angular movement in relation to surface direction normal	23.308	28.23	12.942	17.690	±0.899	±1.960

FIGURE 15. Scenario of the real-world experiment.

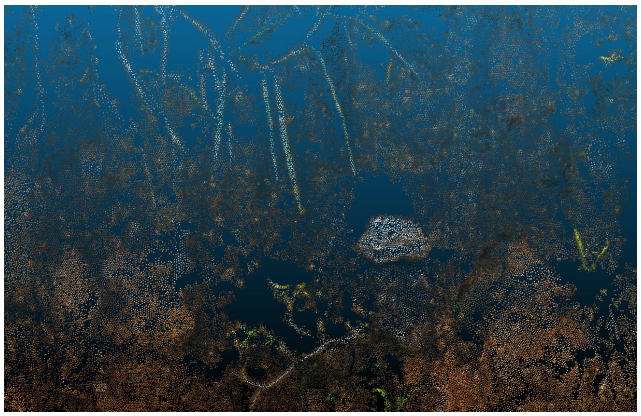

FIGURE 16. SFM reconstruction of the real-world experiment.

FIGURE 17. Representation of the M3C2 displacement as scalar field.

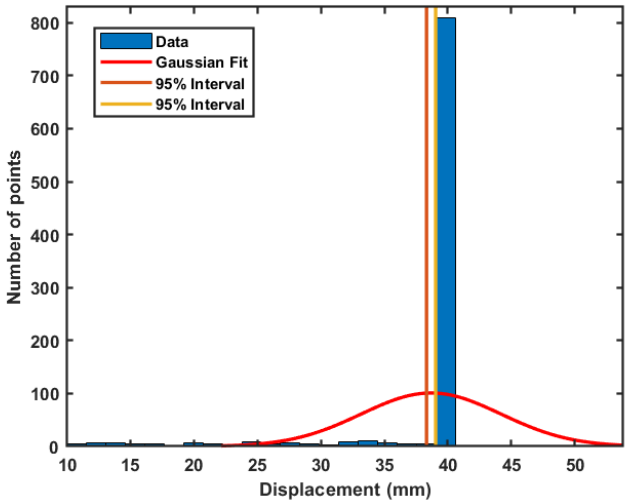

FIGURE 18. M3C2 algorithm histogram of points distances for the movement in the normal direction.

It is observed that the vegetation produces interference, that is, a little amount of red and blue dots distributed over the point cloud. A segmentation method was applied to minimize these influences, removing all vegetation before the analysis of the results. Figure 18 shows the M3C2 result after segmentation.

Figure 19 shows the distance calculation for the proposed method. Note that the algorithm has a good response with similar performance with the M3C2 method. This result demonstrates that the method can be used in real situations.

In a resume, these results showed that M3C2, for instance, is very efficient in detecting changes in the point cloud with a considerably low error if the movement is in the normal direction, which can be seen in the histograms from Figure 10. Note that this is the best condition for M3C2 and similar methods, such as C2C and C2M. When the movement is in different directions from the normal, errors take place. Figure 11 shows the worst-case condition for this type of algorithm. The method detects some changes. However, neither the module of distance and the balance of mass can be trusted. In this situation, the user has to interpret the results

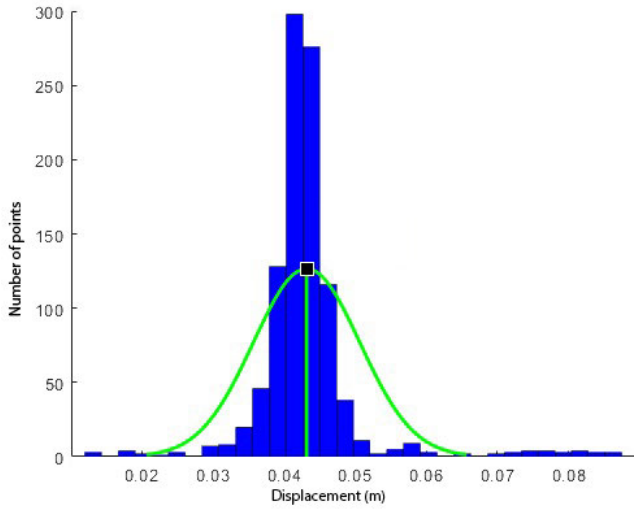

FIGURE 19. 3D-CP2 algorithm histogram of points distances for the movement in the normal direction.

seen in the displacement histograms to understand that the spikes close to zero are actually measurement errors. The last set of histograms are in Figure 13. This experiment shows the middle ground condition, that is, what happens when the movement has an angle (approximately 45 degrees in this case) concerning the normal surface vector.

D. MONITORING OF SOIL EROSION

The next stage is to apply the proof of concept in a real slope subject to erosion. Figure 20 shows the slope used in this experiment. It is important to mention that in many slopes, erosion is the most important force that drives changes and affects the soil profile. The previous sections showed the 3D-CP2 method performance tested in controlled situations. In order to show its robustness, this section presents the proposed method performance evaluation compared with M3C2 without direct comparison with validation measurements. In this experiment, two different reconstructions were built in different epochs to allow comparison. The camera parameters are shown in Table 2 along with reconstruction characteristics. As vegetation can significantly influence the results, most of vegetation was masked and removed after SFM reconstruction.

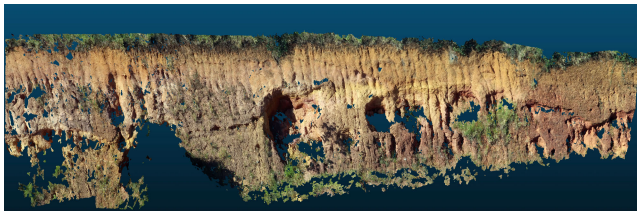

FIGURE 20. Slope subjected to soil erosion.

Both M3C2 and 3D-CP2 methods were applied to the reconstructions to analyze the differences between them.

TABLE 2. Camera and reconstruction parameters.

Camera Parameters		
Resolution	Focal Lenght	Pixel Size
\ 4864 x 3648	8.8 m	2.4 x 2.4 um
Reconstruction Parameters		
Number of points	Max Error	
3697429	3.2 mm	

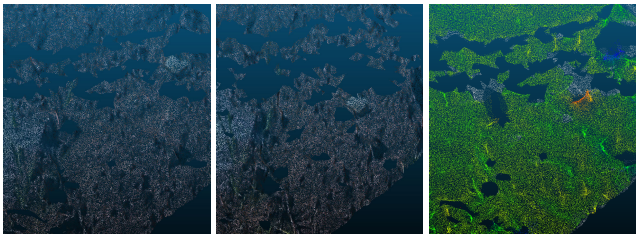

(a) (b) (c)

FIGURE 21. Part of the analysed reconstruction. (a) Before. (b) After. (c) M3C2.

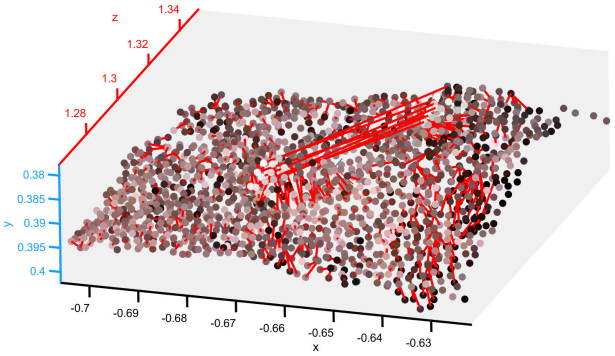

FIGURE 22. Point's movement.

Figure 21 (a) and (b) show the same parts of the reconstruction in different inspection epochs. The whole area has more than 100 meters, and this part was selected to allow better visualization of the moving parts. Figure 21 (c) shows the M3C2 motion estimation between images of Figures 21 (a) and (b).

It is possible to estimate the movements in a structure using the proposed method, as shown in Figure 22. As can be noticed, the motion detected for most parts of the point cloud is related to the difference's in points positions due to 3D reconstruction. However, some points belonging to the reconstruction changing part are showed in proper positions. This result does not happen in the M3C2 results.

The next step is a comparison between the distance measurements for M3C2 and 3D-CP2, as shown in Figure 23 and Figure 24, as also done with other results. It can be noticed that the proposed method shows two groups of points, where one is resultant of SFM errors from points positions, and the second from the real displacement. The M3C2 result also showed a similar displacement. However, the second peak is way closer, and it is related to the loss of mass due to

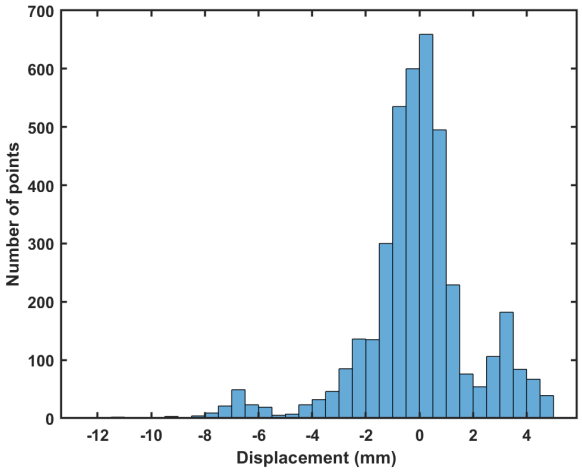

FIGURE 23. Histogram of points distances with an angle in relation to the normal of the surface estimated with 3D-CP2.

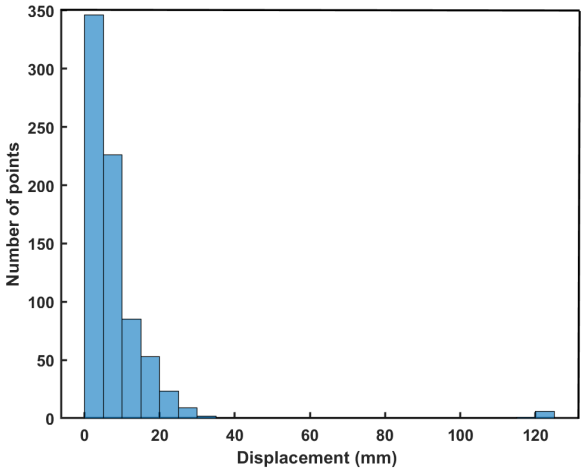

FIGURE 24. Histogram of points distances with an angle in relation to the normal of the surface estimated with M3C2.

the motion in the point cloud. Thus, the result given by the M3C2 does not represent the real displacement observed in the point cloud.

The histograms from Figures 23 and 24 show the displacement distribution for a movement in the normal direction. In this situation, M3C2 and 3D-CP2 should present similar performances. Indeed, this is the result observed in their respective histograms. These results show that the proposed method can be applied in real scenarios.

V. CONCLUSION AND FUTURE WORK

This research proposed a technique to perform alignment and comparison of point clouds. The main purpose of this method is to analyze the point cloud motion to be applied in terrestrial 3D SFM reconstructions. The proposed methodology was used in controlled experiments as well as in real case scenarios to show its potential for point cloud displacements analysis. The results showed that the proposed technique is efficient. Besides, it is capable of surpassing methods that rely on the normal of the surface to compute displacements, such as M3C2.

Despite the authors' promising results, the technique has limitations mainly regarding the computational cost that is higher due to the feature matching process and dependence on feature matching in the image set. Other improvements can be substantial for future works in scenarios that the current techniques are not capable of giving proper results. For example, it is necessary to carry out tests that the registration and scale errors are submillimetric. Therefore, it is also required to use control points more precisely positioned. Another possible improvement would be the combination validation combination of the proposed methodology with the M3C2 technique to provide more correct displacement values and with an associated significance value.

ACKNOWLEDGMENT

The authors would like to thank the CEFET-RJ. This work reported in this paper was performed as part of an interdisciplinary research and development project undertaken by UFJF.

REFERENCES

[1] T. Xu, L. Xu, X. Li, and J. Yao, "Detection of water leakage in underground tunnels using corrected intensity data and 3D point cloud of terrestrial laser scanning," *IEEE Access*, vol. 6, pp. 32471–32480, 2018.

[2] J. Jeon, J. Lee, D. Shin, and H. Park, "Development of dam safety management system," *Adv. Eng. Softw.*, vol. 40, no. 8, pp. 554–563, Aug. 2009.

[3] C. Holst and H. Kuhlmann, "Challenges and present fields of action at laser scanner based deformation analyses," *J. Appl. Geodesy*, vol. 10, no. 1, pp. 17–25, Jan. 2016.

[4] W. Kim, S. Jung, Y. Moon, and S. C. Mangum, "Morphological band registration of multispectral cameras for water quality analysis with unmanned aerial vehicle," *Remote Sens.*, vol. 12, no. 12, p. 2024, Jun. 2020.

[5] P. Ziolkowski, J. Szulwic, and M. Miskiewicz, "Deformation analysis of a composite bridge during proof loading using point cloud processing," *Sensors*, vol. 18, no. 12, p. 4332, Dec. 2018.

[6] Y. S. Hayakawa and H. Obanawa, "Volumetric change detection in bedrock coastal cliffs using terrestrial laser scanning and UAS-based SfM," *Sensors*, vol. 20, no. 12, p. 3403, Jun. 2020.

[7] Z. Zhou, J. Gong, and M. Guo, "Image-based 3D reconstruction for posthurricane residential building damage assessment," *J. Comput. Civil Eng.*, vol. 30, no. 2, Mar. 2016, Art. no. 04015015.

[8] H. Sun, Z. Xu, L. Yao, R. Zhong, L. Du, and H. Wu, "Tunnel monitoring and measuring system using mobile laser scanning: Design and deployment," *Remote Sens.*, vol. 12, no. 4, p. 730, Feb. 2020.

[9] T. Wunderlich, W. Niemeier, D. Wujanz, C. Holst, F. Neitzel, and H. Kuhlmann, "Areal deformation analysis from TLS point clouds—The challenge flächenhafte deformationsanalyse aus tls punktwolken–die herausforderung," Tech. Rep.

[10] B. Jafari, A. Khaloo, and D. Lattanzi, "Deformation tracking in 3D point clouds via statistical sampling of direct cloud-to-cloud distances," *J. Nondestruct. Eval.*, vol. 36, no. 4, p. 65, Dec. 2017.

[11] G. Wang, J. Wu, R. He, and S. Yang, "A point cloud-based robust road curb detection and tracking method," *IEEE Access*, vol. 7, pp. 24611–24625, 2019.

[12] A. Vakhitov and V. Lempitsky, "Learnable line segment descriptor for visual SLAM," *IEEE Access*, vol. 7, pp. 39923–39934, 2019.

[13] Z. Gojcic, C. Zhou, and A. Wieser, "Robust pointwise correspondences for point cloud based deformation monitoring of natural scenes," in *Proc. 4th Joint Int. Symp. Deformation Monit. (JISDM)*, 2019, pp. 1–8.

[14] P. Nesbit and C. Hugenholtz, "Enhancing UAV–SfM 3D model accuracy in high-relief landscapes by incorporating oblique images," *Remote Sens.*, vol. 11, no. 3, p. 239, Jan. 2019.

[15] H. Zhang, E. Aldana-Jague, F. Clapuyt, F. Wilken, V. Vanacker, and K. Van Oost, "Evaluating the potential of post-processing kinematic (PPK) georeferencing for UAV-based structure- from-motion (SfM) photogrammetry and surface change detection," *Earth Surf. Dyn.*, vol. 7, no. 3, pp. 807–827, Sep. 2019.

[16] C. Cabo, C. Ordóñez, F. Sáchez-Lasheras, J. Roca-Pardiñas, and A. J. D. Cos-Juez, "Multiscale supervised classification of point clouds with urban and forest applications," *Sensors*, vol. 19, no. 20, p. 4523, Oct. 2019.

[17] H. Balta, J. Velagic, H. Beglerovic, G. De Cubber, and B. Siciliano, "3D registration and integrated segmentation framework for heterogeneous unmanned robotic systems," *Remote Sens.*, vol. 12, no. 10, p. 1608, May 2020.

[18] N. Ahmad Fuad, A. R. Yusoff, Z. Ismail, and Z. Majid, "Comparing the performance of point cloud registration methods for landslide monitoring using mobile laser scanning data," *ISPRS Int. Arch. Photogramm., Remote Sens. Spatial Inf. Sci.*, vol. XLII-4/W9, pp. 11–21, Oct. 2018.

[19] H. Neuner, C. Holst, and H. Kuhlmann, "Overview on current modelling strategies of point clouds for deformation analysis," *Allg. Vermess. Nachr.(AVN)*, vol. 123, pp. 328–339, Nov. 2016.

[20] R. Qin, J. Tian, and P. Reinartz, "3d change detection–approaches and applications," *ISPRS J. Photogramm. Remote Sens.*, vol. 122, pp. 41–56, Dec. 2016.

[21] P.-M. DiFrancesco, D. Bonneau, and D. J. Hutchinson, "The implications of M3C2 projection diameter on 3D semi-automated rockfall extraction from sequential terrestrial laser scanning point clouds," *Remote Sens.*, vol. 12, no. 11, p. 1885, Jun. 2020.

[22] M. R. James, S. Robson, and M. W. Smith, "3-D uncertainty-based topographic change detection with structure-from-motion photogrammetry: Precision maps for ground control and directly georeferenced surveys," *Earth Surf. Processes Landforms*, vol. 42, no. 12, pp. 1769–1788, 2017.

[23] C. Zhou, F. Li, and W. Cao, "Architecture design and implementation of image based autonomous car: THUNDER-1," *Multimedia Tools Appl.*, vol. 78, no. 20, pp. 28557–28573, Oct. 2019.

[24] Y. Pan, Y. Han, L. Wang, J. Chen, H. Meng, G. Wang, Z. Zhang, and S. Wang, "3D reconstruction of ground crops based on airborne LiDAR technology," *IFAC-PapersOnLine*, vol. 52, no. 24, pp. 35–40, 2019.

[25] N. Qin, X. Hu, and H. Dai, "Deep fusion of multi-view and multimodal representation of ALS point cloud for 3D terrain scene recognition," *ISPRS J. Photogramm. Remote Sens.*, vol. 143, pp. 205–212, Sep. 2018.

[26] E. Menendez, J. G. Victores, R. Montero, S. Martínez, and C. Balaguer, "Tunnel structural inspection and assessment using an autonomous robotic system," *Autom. Construct.*, vol. 87, pp. 117–126, Mar. 2018.

[27] R. Lindenbergh and P. Pietrzyk, "Change detection and deformation analysis using static and mobile laser scanning," *Appl. Geomatics*, vol. 7, no. 2, pp. 65–74, Jun. 2015.

[28] L. Fan, "A comparison between structure-from-motion and terrestrial laser scanning for deriving surface roughness: A case study on A sandy terrain surface," *Int. Arch. Photogramm., Remote Sens. Spatial Inf. Sci.*, vol. 42, pp. 1225–1229, Feb. 2020.

[29] N. Wang, Y. Zhang, Z. Li, Y. Fu, H. Yu, W. Liu, X. Xue, and Y.-G. Jiang, "Pixel2Mesh: 3D mesh model generation via image guided deformation," *IEEE Trans. Pattern Anal. Mach. Intell.*, early access, Apr. 2, 2020, doi: 10.1109/TPAMI.2020.2984232.

[30] H. Zhu, B. Guo, K. Zou, Y. Li, K.-V. Yuen, L. Mihaylova, and H. Leung, "A review of point set registration: From pairwise registration to groupwise registration," *Sensors*, vol. 19, no. 5, p. 1191, Mar. 2019.

[31] J. Han, P. Yin, Y. He, and F. Gu, "Enhanced ICP for the registration of large-scale 3D environment models: An experimental study," *Sensors*, vol. 16, no. 2, p. 228, Feb. 2016.

[32] J. Park, Q.-Y. Zhou, and V. Koltun, "Colored point cloud registration revisited," in *Proc. IEEE Int. Conf. Comput. Vis. (ICCV)*, Oct. 2017, pp. 143–152.

[33] X. Ren, M. Zhang, W. Wang, X. Mao, and J. Ren, "Fast and coarse registration of point cloud in ICP three-dimensional space," *J. Phys., Conf. Ser.*, vol. 1453, Jan. 2020, Art. no. 012023.

[34] X. Shi, T. Liu, and X. Han, "Improved iterative closest Point(ICP) 3D point cloud registration algorithm based on point cloud filtering and adaptive fireworks for coarse registration," *Int. J. Remote Sens.*, vol. 41, no. 8, pp. 3197–3220, Apr. 2020.

[35] S. Bouaziz, A. Tagliasacchi, and M. Pauly, "Sparse iterative closest point," in *Proc. 11th Eurographics/ACMSIGGRAPH Symp. Geometry Process.*, 2013, pp. 113–123.

[36] J. Bedkowski, M. Pełka, K. Majek, T. Fitri, and J. Naruniec, "Open source robotic 3D mapping framework with ROS—Robot operating system, PCL—Point cloud library and cloud compare," in *Proc. Int. Conf. Electr. Eng. Informat. (ICEEI)*, 2015, pp. 644–649.

[37] A. Wagner, W. Wiedemann, and T. Wunderlich, "Fusion of laser-scan and image data for deformation monitoring–concept and perspective," in *Proc. 7th Int. Conf. Eng. Surveying (INGEO)*, 2017, pp. 157–164.

[38] D. Rethage, J. Wald, J. Sturm, N. Navab, and F. Tombari, "Fully-convolutional point networks for large-scale point clouds," in *Proc. Eur. Conf. Comput. Vis. (ECCV)*, 2018, pp. 596–611.

[39] B. Lin, "Change detection of 3D scene with 3D and 2D information for environment checking," Ph.D. dissertation, Dept. Inf. Eng., Hiroshima Univ., Higashihiroshima, Japan, 2013.

[40] D. Lague, N. Brodu, and J. Leroux, "Accurate 3D comparison of complex topography with terrestrial laser scanner: Application to the Rangitikei canyon (N-Z)," *ISPRS J. Photogramm. Remote Sens.*, vol. 82, pp. 10–26, Aug. 2013.

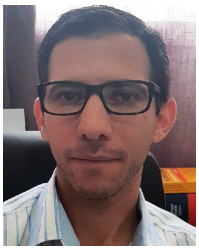

AURELIO G. MELO (Member, IEEE) received the bachelor's degree in information systems from Presidente Antonio Carlos University and the master's degree in agricultural engineering from the Federal University of Viçosa (UFV). He is a Control and Automation Engineer with the Federal Center of Technological Education of Minas Gerais (CEFET-MG). He has experience in both industrial and academic areas. He holds an academic internship at the company of Alternativa Eletrica, Uba, Brazil, in the automation and panel assembly sector. He was a Professor at the SENAI, Uba. He is currently a Subsea Control Systems Technician with Schlumberger, Brazil.

MILENA F. PINTO (Member, IEEE) received the master's and Ph.D. degrees in electrical engineering from the Federal University of Juiz de Fora (UFJF), with one year of doctoral research at the Technische Universität München. She is a Control and Automation Engineer with the Federal Technological Education Center of Minas Gerais-CEFET/MG. She has experience in both industrial and research areas. She did an academic internship at the Institute of Combustion Technology, German Aerospace Center (DLR), Stuttgart, Germany. She has also worked as a Trainee Engineer at TELNAV Telecomunicacoes Navais, Macaé, Brazil. She is currently a Professor with the Centro Federal de Educação Tecnológica Celso Suckow da Fonseca (CEFET/RJ) and a Researcher with the Energy Department of the Electrical Engineering of UFJF. Her research interests include artificial intelligence, robotic systems, unmanned aerial vehicles, and fog-cloud computing.

LEONARDO M. HONÓRIO received the B.Sc. degree from the Federal University of Juiz de Fora (UFJF) in 1993, and the M.Sc. and Ph.D. degrees from the EFEI, Brazil, in 1999 and 2002, respectively, all in electrical engineering. He was a Visiting Researcher with Porto and Irvine California University, in 2006 and 2012, respectively. He is currently a Full Professor with the UFJF. His current research interests include evolutionary algorithms, probabilistic methods, optimal power flow, robotics, autonomous vehicles, fuzzy logic, control, pattern recognition, and optimization.

FELIPE M. DIAS received the degree in electrical engineering with an emphasis on electronic systems from the Federal University of Juiz de Fora (UFJF), with one year at the Illinois Institute of Technology, Chicago, USA. He is currently pursuing the master's degree in electrical engineering with the Intelligent Robotics Group (GRIn), UFJF, working in the computer vision area to monitor large structures (dams and embankments). He participated in a scientific initiation project focusing on electronic instrumentation using the LabVIEW software. He carried out a project on the generation of three-dimensional visual and thermal models for electrical equipment using computer vision techniques. Besides, he also participates in biomedical signal processing work using techniques such as machine learning and compressive sampling.

JULIANO E. N. MASSON is currently pursuing the master's degree in control and automation engineering with the Federal University of Santa Catarina (UFSC). He is a Control and Automation Engineer with the Federal University of Santa Catarina (UFSC). He has experience in multi-view stereo, LIDAR, 3D data, and meshing/texturization algorithms.